Research Article

Lu Tang#, Wanli Liu#, Xinyi Wang#, Yu Li, Hai Lan, Guohua Wu, and Zhihong Dong*

Electrospinning of MNZ/PLGA/SF nanofibers for periodontitis

https://doi.org/10.1515/ntrev-2024-0091
received December 27, 2023; accepted July 28, 2024

Abstract: In this study, the electrospinning technique was employed to create a nanofiber membrane by stretching an organic polymer into nanofibers under a high electric field. Metronidazole (MNZ) at a concentration of 3 wt% was loaded into a poly(lactic-co-glycolic acid) (PLGA) and silk fibroin (SF)-blended nanofiber membrane. This formulation aims to achieve effective and sustained drug release, enabling the eradication of bacteria for the efficient treatment of periodontitis. Results demonstrated that SF interacted with PLGA molecules, forming dense and uniform nanofibers with a diameter of 570 nm. Excessive SF molecules tended to aggregate, leading to an increased particle size, with the interaction between MNZ and SF contributing to adhesion. The composition of MNZ, SF, and PLGA formed a physical chimera without any chemical reactions. Moreover, as the SF content increased, the tensile properties of the membrane gradually improved. Concurrently, the *in vitro* degradation rate increased with higher SF content. Among the various groups tested, the 3 wt% MNZ/PLGA/SF 2:1 membrane exhibited superior drug release characteristics, with 71.76% release within 24 h. This formulation demonstrated excellent antibacterial properties, indicated by a bacterial inhibition diameter of 13.5 mm, noteworthy hydrophilicity with a contact angle of 44.3°, and favorable biocompatibility. The membrane holds significant application value in regenerative engineering and drug delivery systems, showcasing substantial potential for the treatment of periodontitis.

Keywords: electrospinning, poly(lactic-co-glycolic acid), silk fibroin, metronidazole, nanofibers membrane

1 Introduction

Periodontitis stands as a chronic inflammatory and destructive oral disease primarily characterized by the formation of plaque beneath the gingiva [1]. The pathogenesis of periodontitis involves the gradual erosion of periodontal tissue integrity by the host's immune system and bacterial infection, potentially leading to the absorption of alveolar bone and loss of periodontal ligament attachment [2]. This progressive process results in the loosening of teeth and, ultimately, tooth loss. The primary objective of early periodontal treatment is to control inflammation and prevent the further progression of periodontitis [3]. The success of periodontal treatment crucially hinges on the judicious selection of the right antibacterial drug and the appropriate route of administration [4]. The main pathogenic bacteria of periodontitis are anaerobic bacteria, and *Escherichia coli* is also one of the pathogenic bacteria. Metronidazole (MNZ) emerges as a fitting antimicrobial agent for the treatment of periodontitis. With its nitro structure, it actively participates in the energy metabolism of bacteria, disrupting the structure of genetic material (DNA), and inhibiting DNA synthesis. This interference effectively disrupts the growth and reproduction of pathogenic microorganisms, thereby exerting a sterilizing effect [5]. MNZ demonstrates potent bactericidal effects against bacteria [6].

In clinical practice, oral antibiotics are typically prescribed for 3–5 days as part of systemic treatment. This approach necessitates administering a sufficiently high dosage to the pocket area to attain the required concentration [7]. However, prolonged or excessive antibiotic use can lead to adverse reactions, including nausea, loss of appetite, abdominal cramps, headache, and dizziness [8]. To optimize therapeutic outcomes while minimizing adverse effects, local administration is often preferred [9]. This involves

# These authors contributed equally to this work and should be considered first co-authors.

* **Corresponding author: Zhihong Dong,** Affiliated Hospital and Clinical College, School of Mechanical Engineering, Chengdu University, Chengdu, 610106, China, e-mail: zhdong@cdu.edu.cn
Lu Tang, Wanli Liu, Yu Li, Hai Lan: Affiliated Hospital and Clinical College, School of Mechanical Engineering, Chengdu University, Chengdu, 610106, China
Xinyi Wang: Department of Urology and Institute of Urology, West China Hospital, Sichuan University, Chengdu, 610065, China
Guohua Wu: National Engineering Research Center for Biomaterials, Sichuan University, Chengdu, 610065, China

loading antibacterial drugs onto a membrane, allowing for the gradual release of drug components into the periodontal pocket [10,11]. The key challenge is to maintain a sufficiently high concentration of antibacterial drugs in the periodontal pocket for an adequate duration to effectively treat periodontitis [12]. This controlled and sustained release strategy aims to eradicate bacteria while minimizing adverse effects on the body [13]. Poly(lactic-co-glycolic acid) (PLGA), a degradable synthetic polymer, boasts excellent biocompatibility and membrane-forming capabilities, making it a versatile material in pharmaceutical and biomedical applications [14,15]. PLGA-loaded nanofiber membranes with different substances were studied for periodontitis by electrospinning [16,17]. However, the strong hydrophobicity of PLGA is not conducive to the adhesion properties of periodontal barrier membranes. Meanwhile, silk fibroin (SF), primarily extracted from silkworms, is a natural polymer known for its biocompatibility, biodegradability, morphological flexibility, mechanical properties, low inflammatory response, and non-toxicity [18,19]. Therefore, synthetic polymers incorporated with natural polymers may not only enhance hydrophilicity [20] but also have better biocompatibility and could improve the cell affinity [21].

In this study, a biomembrane drug delivery system for treating periodontitis was designed, consisting of a PLGA/SF nanofiber membrane loaded with MNZ *via* electrospinning. Electrospinning is a versatile technique that enables the production of nanofibers with unique properties [22]. The polymer solution is sprayed and ejected in a strong electric field, where the droplets at the tip of the needle transform from a spherical shape to a conical shape. Eventually, a nanofiber film is collected on a metal collector [23]. The membrane's forming properties, hydrophilicity, and mechanical characteristics were tailored by adjusting the PLGA and SF ratio. This nanofiber membrane serves a dual purpose: controlling the drug release and facilitating absorption by surrounding tissues, ensuring a continuous release of MNZ to effectively combat bacteria and achieve the desired therapeutic effect in treating periodontitis.

2 Materials and methods

2.1 Materials

PLGA, with an analytical grade and a molecular weight of 100,000–120,000 Da, sourced from Daigang Bioengineering Co., Ltd., Jinan, Shandong, China; SF obtained from Sichuan Antibiotics Research Institute; MNZ also sourced from Sichuan Antibiotics Research Institute; hexafluoroisopropanol (HFIP) with a purity of 99.5% obtained from Adamas; osteoblasts (MC3T3-E1) acquired from the Chinese Academy of Sciences Cell Bank; and phosphate-buffered saline obtained from Feijing Biotechnology Co., Ltd.

2.2 Preparation of nanofiber membrane

PLGA was dissolved in HFIP at 15 wt% and ultrasonic for 1 h to obtain a clear yellow solution. The solution mixed with MNZ (3 wt%), and different ratio of SF (2:1 and 1:1), and pure PLGA solution as control, respectively [24]. Four milliliters of different solutions was put into a 10 ml syringe and fixed to the pusher of the electrospinning machine. A clip was attached to the needle of the syringe. The distance between the needle and the receiving roller was 20 cm, the voltage was 15 kV, the feed rate was 0.0025 mm/s, and the ambient temperature was 25°C. Pure PLGA membrane, 3 wt% MNZ/PLGA membrane, PLGA/SF 2:1 membrane, PLGA/SF 1:1 membrane, 3 wt% MNZ/PLGA/SF 2:1 membrane, and 3 wt% MNZ/PLGA/SF 1:1 membrane were fabricated and dried in a freeze dryer for 24 h and stored at 4°C.

2.3 Surface morphology

A 1 cm × 1 cm sample underwent gold sputtering for 50 s to enhance conductivity. The surface morphology, uniformity, and structure of the nanofibers were examined using scanning electron microscopy (SEM) at an acceleration voltage of 20 kV under vacuum conditions (HITACHI SU8010, Japan). To determine the average diameter, 20 randomly selected fibers were measured from SEM images, and ImageJ software was utilized for the analysis.

2.4 Contact angle

The contact angle of the nanofiber composite membrane was determined using a contact angle meter (LSA60, Germany). Three distinct points were measured for each sample. Following exposure to room temperature for 10 s, the water droplet's image on the sample surface was captured by a camera and subsequently analyzed using the software provided by the manufacturer.

2.5 Fourier transform infrared (FTIR) spectroscopy

The functional groups of the nanofiber composite membrane were detected in the range of 400–3,500 cm^{-1} using an FTIR spectrophotometer (Tensor ll, Germany).

2.6 Mechanical properties

The prepared membrane was trimmed to dimensions of 5 cm in length and 1 cm in width, with a measured thickness of 0.04 mm using a screw micrometer. Tensile strength testing was conducted on a tensile strength testing machine (APLY-103, Huitai Machinery Co., Ltd., Dongguan, China) at a stretching speed of 10 mm/min. Each sample group underwent three stretching trials, and the average value was computed to determine the tensile strength.

2.7 Thermogravimetric analysis (TGA)

A 5 mg sample was introduced into an alumina crucible and subjected to testing in a nitrogen atmosphere with a heating rate of 10°C/min within the temperature range of 25–100°C. The thermal stability of the sample was assessed through TGA, and the thermogravimetric curve of the nanofiber composite membrane, spanning from room temperature to 600°C, was recorded. Differential treatment of the thermogravimetric curve was then conducted to identify the temperature range associated with rapid decomposition from the curve.

2.8 Water absorption

A 10 mg (M_0) sample was immersed in phosphate buffer for 1, 3, 6, and 24 h, respectively, at 37°C in a water bath. The samples were labeled and taken out at the specified time. The composite membrane surface was carefully dried with filter paper and weighed (M_1). The experiment was repeated three times. The water absorption of the nanofiber composite membrane was calculated by the following equation:

$$\text{Water absorption} = (M_1 - M_0)/M_0 \times 100\% \ (n = 3)$$

2.9 *In vitro* degradation testing

A 10 mg sample was immersed in phosphate buffer for 1, 3, 5, 7, 14, and 21 days, respectively, at 37°C in a water bath. The samples were labeled and taken out at the specified time. The samples were dried and weighed. The experiment was repeated three times.

2.10 Cytocompatibility

Osteoblast cells (MC3T3-E1) were seeded in 96-well plates at a density of 2×10^3 cells per well and cultured. Each sample occupied a 1 cm × 1 cm area. Following the manufacturer's instructions, cell viability was assessed using a cell counting Kit-8 (CCK-8) kit at 1 and 3 days of culture. At the end of each time point, the cell culture medium was replaced. After incubating the cells with fresh culture medium containing CCK-8 reagent (1:10) at 37°C for 1 h, absorbance was measured at a wavelength of 450 nm using spectrophotometry and an enzyme-linked immunosorbent assay microwell plate reader (Epoch2, BIO-TEK, USA).

2.11 Encapsulation efficiency

The drug-loaded nanofiber membrane (10 mg) was completely dissolved in 1 ml HFIP, and methanol was added to achieve a volume of 10 ml. The mixture was sonicated for 2 h, the supernatant was separated by centrifugation, and the characteristic peak value of MNZ was obtained at 320 nm by ultraviolet spectrophotometer. The encapsulation efficiency of drug-loaded nanofiber membrane was calculated by the following formula:

$$\text{Encapsulation efficiency (\%)} = \text{actual drug amount (mg)} / \text{theoretical drug amount (mg)}.$$

2.12 Drug release

A 10 mg sample of the loaded membrane was weighed using an electronic balance. The dried loaded membrane was introduced into a beaker containing 15 ml of phosphate buffer solution. The beaker's opening was sealed with plastic wrap, and it was positioned in a constant-temperature magnetic stirring water bath. A magnet was included to facilitate solution stirring, and the parameters were set to 37°C for 24 h. One milliliter of the solution was taken at 1, 3, 6, and 24 h, and 1 ml of phosphate buffer was immediately added to the beaker to adjust the pH to 7.2–7.4. The extracted 1 ml solution was placed in a cuvette, and absorbance was measured at a wavelength of 320 nm using a UV spectrophotometer. Corresponding absorbance values were obtained for known concentrations, and a standard curve was generated. The percentage of drug released was then calculated based on the initial weight of the drug in the drug-carrying membrane.

2.13 Antibacterial test

In the antibacterial assay, disposable inoculation rings, coated rods, and glass tubes were sterilized using UV

irradiation. Bacteria were extracted using an inoculation ring, dissolved in deionized water in a glass test tube, mixed evenly, and then placed in the medium. *E. coli*, a Gram-negative and facultative anaerobic bacteria, is also one of the pathogenic bacteria of periodontitis. The medium's surface was evenly coated with a coating rod. Three zones were created on the medium's surface, and samples with a diameter of 8 mm, including PLGA, PLGA/SF 2:1, and 3 wt% MNZ/PLGA/SF 2:1, were placed on these zones. The medium was subsequently incubated in a bacterial incubator for 24 h. Antibacterial activity was evaluated by measuring the area of the antibacterial zone.

3 Results and discussion

3.1 Surface morphology

The surface morphology of the membranes is detailed in Figure 1, where distinctive features of pure PLGA, 3 wt% MNZ/PLGA, two variants of PLGA/SF, and two types of PLGA/SF-loaded membranes with 3 wt% MNZ are revealed. The pure PLGA membrane exhibits uniform size and good dispersion, with an average diameter of 310 nm. However, in the case of 3 wt% MNZ/PLGA, the diameter size increases to 420 nm. The elevated MNZ content in the spinning solution enhances solution viscosity, leading to increased fiber diameter and the occurrence of adhesion. High-viscosity solutions hinder the stretching of the polymer jet, causing enlarged droplet diameters at the needle tip, resulting in the formation of beaded fibers. SF, a high molecular weight fibrous protein, is blended with PLGA and interacts with PLGA molecules. The interaction prompts protein molecules to transition from a swollen to a compact state, wrapping internal hydrophilic groups and exposing hydrophobic groups [25]. This results in the formation of dense and uniform nanofibers. In PLGA/SF 1:1, the average diameter increases to 730 nm, showcasing significantly larger fiber diameters and the appearance of partial aggregates [26]. Excessive SF molecules can adhere to each other, forming aggregates with increased size. The average diameter of 3 wt% MNZ/PLGA/SF 2:1 is 640 nm, while that of 3 wt% MNZ/PLGA/SF 1:1 is 930 nm. The interaction between MNZ and SF contributes to adhesion. MNZ is attached to the nanofibers in the form of solid particles. The appropriate concentration of MNZ has good porosity, and the overall structure is an interpenetrating network, which provides enough space for cell nutrient exchange and drug release.

3.2 Contact angle

The contact angles of pure PLGA, 3 wt% MNZ/PLGA, two groups of PLGA/SF with different ratios, and two groups of PLGA/SF-loaded membranes with 3 wt% MNZ are shown in Figure 1. The wettability of the material surface can be judged by the contact angle [27]. The contact angle of pure PLGA is 117.8 ± 0.2°, indicating that it is hydrophobic. As the hydrophilic SF is continuously added, the contact angle becomes smaller, and the hydrophilicity gradually increases. Through the experimental results, it can be verified that SF is a hydrophilic material. With the addition of 3 wt% MNZ, the contact angle also becomes smaller, and the hydrophilicity further increases. The contact angle of 3 wt% MNZ/PLGA/SF 1:1 reaches 29.5 ± 0.8° compared with PLGA/SF 1:1 of 56.6 ± 0.8°. Hydrophilic groups including amino acid and hydrogen bonds of SF in the fiber membranes have a great influence on the wettability of the fiber [28]. The addition of water-soluble MNZ and the special structure of SF can effectively adjust the hydrophilicity and hydrophobicity of the composite membrane. Good hydrophilic membranes facilitate cell growth and proliferation in contact with body fluids.

3.3 FTIR spectroscopy

The infrared spectra of pure PLGA, 3 wt% MNZ/PLGA, two groups of PLGA/SF, and two groups of PLGA/SF loaded membranes with 3 wt% MNZ are shown in Figure 2(a). In the spectrum of PLGA, symmetric and asymmetric C–O–C stretching peaks appear at 1,088 and 1,187 cm^{-1}, respectively, and the C═O stretching peak appears at 1,755 cm^{-1} [29]. These stretching peaks are also observed in all the prepared membranes. In the spectrum of MNZ, C–N stretching peak appears at 823 cm^{-1}, N═O stretching peak appears at 1,365 cm^{-1}, and C═C stretching peak appears at 1,537 cm^{-1}. In the 3 wt% MNZ/PLGA fiber membranes, the characteristic peaks of MNZ functional groups are all obvious, and no any shift. Meanwhile, no new peaks are produced, indicating that no new chemical bonds are formed. This is consistent with physical adsorption and embedding. In the spectrum of SF, phenylalanine stretching peak appears at 1,616 cm^{-1} [30], amide I stretching peak appears at 1,688 cm^{-1}, and N–H stretching peak appears at 3,282 cm^{-1}. These stretching peaks are also observed in PLGA/SF 2:1 and PLGA/SF 1:1. With increasing SF content, the characteristic peaks of functional groups become more obvious and no new peaks are produced, indicating that no new chemical bonds are formed. In the blends of MNZ/PLGA/SF, these characteristic peaks

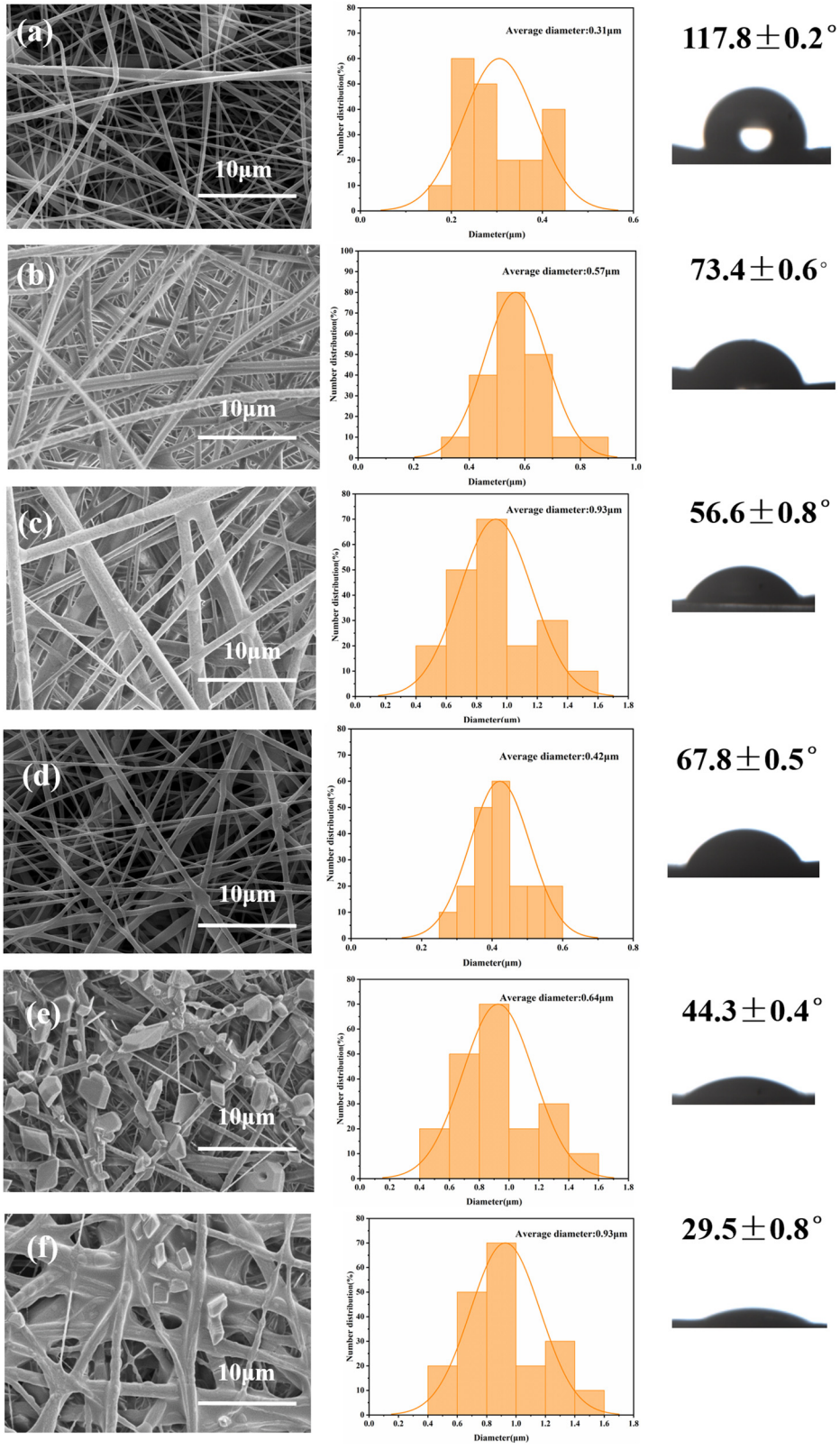

Figure 1: Electron microscopic observation, particle size, and contact angle of nanofibrous membranes with different compositions: (a) PLGA; (b) PLGA/SF 2:1; (c) PLGA/SF 1:1; (d) 3 wt% MNZ/PLGA; (e) 3 wt% MNZ/PLGA/SF 2:1; and (f) 3 wt% MNZ/PLGA/SF 1:1.

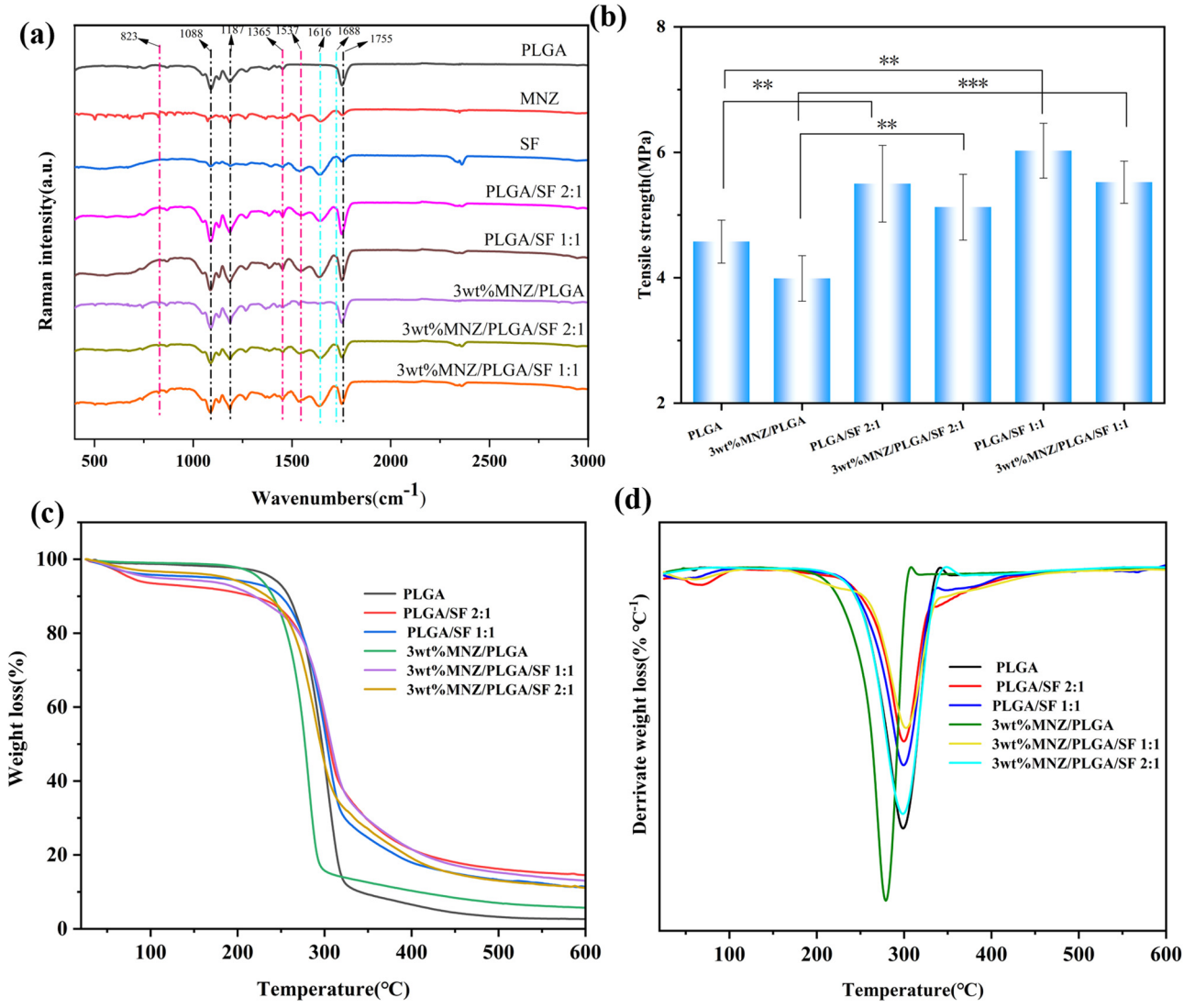

Figure 2: Characterization of nanofibrous membranes with different compositions: (a) Fourier infrared; (b) tensile testing; (c) thermogravimetric analysis (TGA); and (d) derivative thermogravimetric (DTG) analysis.

show better composition of MNZ, PLGA, and SF, which is consistent with physical adsorption and embedding.

3.4 Mechanical properties

The tensile strength of pure PLGA, 3 wt% MNZ/PLGA, two groups of PLGA/SF with different ratios, and two groups of PLGA/SF loaded membranes with 3 wt% MNZ are shown in Figure 2(b). The tensile strength of the pure PLGA membrane is 4.58 MPa, and the tensile strength of 3 wt% MNZ/PLGA membranes is 3.99 MPa. The tensile strengths of PLGA/SF 2:1 and PLGA/SF 1:1 are 5.53 and 6.03 MPa, respectively. The tensile strengths of 3 wt% MNZ/PLGA/SF 2:1 and 3 wt% MNZ/PLGA/SF 1:1 are 5.12 and 5.52 MPa, respectively. From the analysis of the three groups of MNZ/PLGA-loaded membranes with different concentrations of SF, it can be seen that as the loading MNZ, the tensile strength all decreases relative to no loading MNZ. This may be due to the weakness of the clusters of MNZ in the polymer matrix, which are easily ruptured when subjected to stress, thereby reducing the strength of the loaded membrane [31]. From the analysis of the two groups of PLGA/SF with different ratios, it can be seen that SF has good mechanical properties. As the amount of SF increases, the tensile strength is significantly enhanced. The ratio of SF and MNZ can be effectively adjusted to improve the mechanical properties of the composite membrane. Good mechanical properties can ensure the stability of the nanofiber membrane and simulate the characteristics of natural extracellular matrix, which

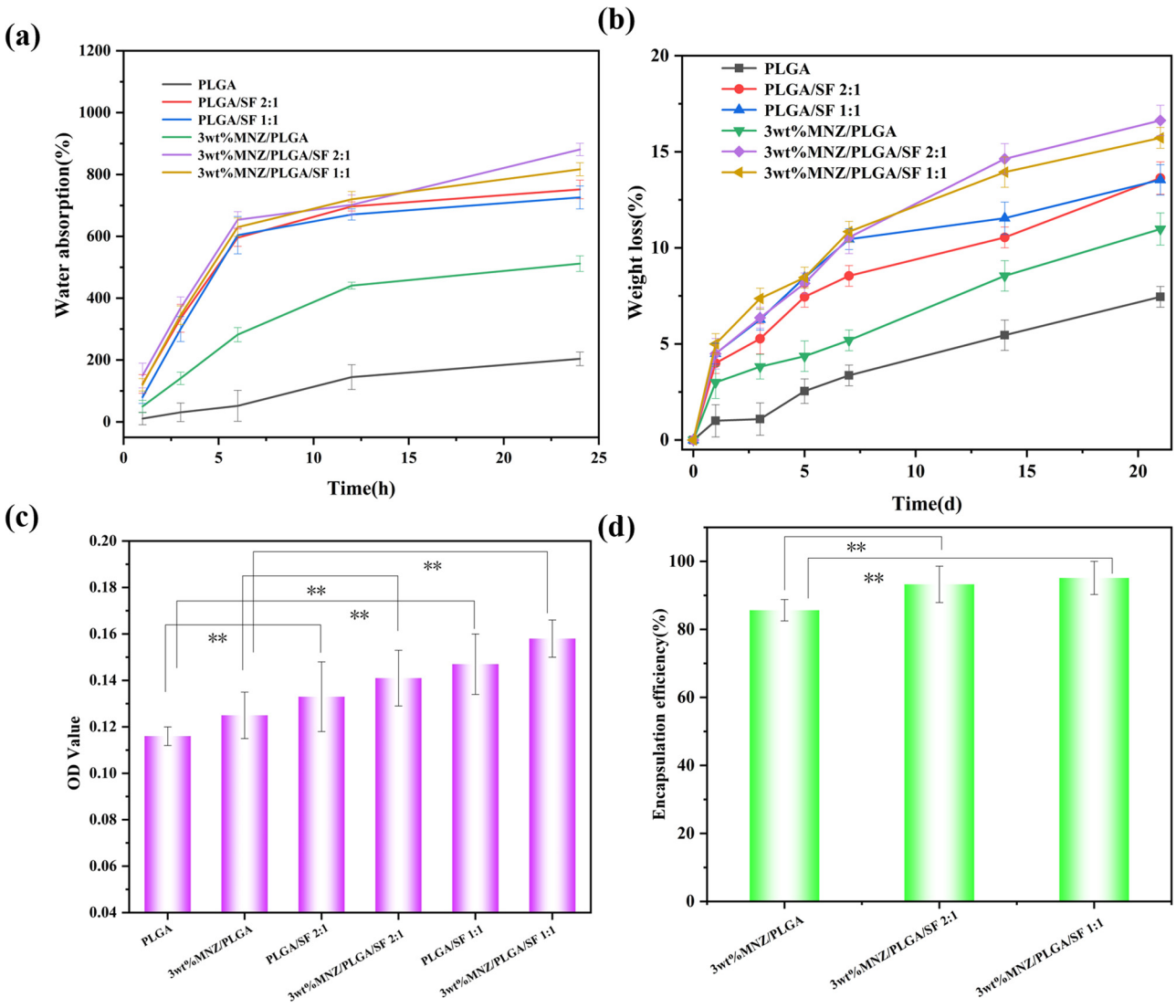

Figure 3: Evaluation of nanofibrous membranes with different compositions. (a) water absorption; (b) *in vitro* degradation; (c) biocompatibility; and (d) encapsulation efficiency.

provide good conditions for the growth and proliferation of osteoblasts, and are conducive to the induction of alveolar bone regeneration.

3.5 TGA

TGA and derivative thermogravimetric analysis of pure PLGA, 3 wt% MNZ/PLGA, two groups of PLGA/SF with different ratios, and two groups of PLGA/SF-loaded membranes with 3 wt% MNZ are shown in Figure 2(c) and (d). The initial degradation temperature of PLGA thermal degradation is about 234°C, and the decomposition rate is the fastest at 316°C. The complete degradation occurs at 400°C. When MNZ is added, the degradation temperature is slightly reduced, with a reduction range of 30°C. SF is a natural polymer compound. Under high-temperature conditions, the thermal motion of organic matter molecules is intensified, and the bond energy inside the molecules is destroyed, leading to the rupture and recombination of molecules. In this process, the carbon content gradually increases and is gradually converted into carbonaceous substances [32,33]. When SF is blended with PLGA, it decomposes to a certain extent above 50°C. As the amount of SF increases, the weight loss platform from 92 to 203°C becomes more obvious. The basic trend remains unchanged after adding 3 wt% MNZ. It can be concluded this composite membrane had good thermal stability.

3.6 Water absorption

The water absorption of pure PLGA, 3 wt% MNZ/PLGA, two groups of PLGA/SF, and two groups of PLGA/SF-loaded membranes with 3 wt% MNZ are shown in Figure 3(a). With the prolong of time, the water absorption rate of each group gradually increased. When added into MNZ, 3 wt% MNZ/PLGA has water absorption of 5.12 times than PLGA of 2.04 times after 24 h. The contact angle experiment has approved that MNZ has good hydrophilicity. After adding SF, the water absorption of PLGA/SF 2:1 is 5.96, 6.97, and 7.52 times in 6, 12, and 24 h, respectively, showing significant improvement due to high-molecular weight globular protein of SF with a high content of hydrophilic groups on its branch chain [34,35]. When SF increases, the water absorption of PLGA/SF 1:1 is 6.04, 6.71, and 7.26 times in 6, 12, and 24 h, respectively. The water absorption does not increase significantly compared to PLGA/SF 2:1, which may be due to the uneven distribution of nanofiber diameter and greater viscosity of excessive SF in the electrospinning process, which affects the water absorption [36]. The molecular structure of SF contains a β-fold structure, forming a stable hydrogen bond to attract more water molecules with the polar hydroxyl and carboxyl groups in the SF, and further improving the water absorption rate. The water absorption of 3 wt% MNZ/PLGA/SF 2:1 is 6.54, 7.02, and 8.81 times in 6, 12, and 24 h, which is superior to 3 wt% MNZ/PLGA/SF 1:1 of 6.3, 7.2, and 8.17 times. MNZ is evenly dispersed on the nanofiber membrane with good porosity, which increases the area of contact with water. The synergistic effect of MNZ and SF further enhances the water absorption, but more SF aggravates the adhesion of nanofibers, reducing the pore volume and affecting the water absorption [37].

3.7 *In vitro* degradation testing

The *in vitro* degradation of pure PLGA, 3 wt% MNZ/PLGA, and two groups of PLGA/SF loaded membranes with 3 wt% MNZ are shown in Figure 3(b). As can be seen from the figure, the weight continues to decrease with the prolongation of degradation time. The loaded composite membranes have a higher degradation rate than the pure PLGA membrane in the first 7 days, and the weight loss rate is also higher than the pure PLGA membrane after 21 days [38]. Pure PLGA was degraded by 7.45%, and 3 wt% MNZ/PLGA was degraded by 13.63%. This trend suggests that the addition of MNZ accelerates the degradation of PLGA membranes. This is because part of the MNZ is attached to the surface of the membrane during the electrospinning process. When the membrane comes into contact with the buffer solution, the drug can quickly and directly diffuse into the buffer solution, increasing the weight loss rate of the membrane [39]. At the same time, because MNZ is a hydrophilic substance, it also promotes degradation. The PLGA/SF composite membranes have a higher degradation rate than the pure PLGA membrane with a prolong time from 7 to 21 days [40]. The degradation rate of PLGA/SF 2:1 was 13.54%, and that of PLGA/SF 1:1 was 10.98%. This trend suggests that the addition of SF accelerates the degradation of PLGA membranes [41]. SF is a highly hydrophilic substance, which promotes the absorption of the membrane, and the aqueous medium penetrates into the polymer matrix, causing the polymer chain to relax, the ester bond to start to hydrolyze, the molecular weight to decrease, and gradually degrade into low molecular weight polymers. The weight loss of PLGA/SF 1:1 is similar to that of PLGA/SF 2:1, which may be because excessive SF causes serious adhesion of nanofibers, hindering *in vitro* degradation. The nanofibers are cohesive in structure, and the internal ester bond is not easy to break, which hinders the degradation of the material *in vitro* to a certain extent. The weight of 3 wt% MNZ/PLGA/SF 2:1 was reduced to 16.63% degradation, and that of 3 wt% MNZ/PLGA/SF 1:1 was 15.73% degradation. This shows that the synergistic effect of MNZ and SF greatly promotes the degradation rate.

3.8 Biocompatibility

The biocompatibility of pure PLGA, 3 wt% MNZ/PLGA, two groups of PLGA/SF, and two groups of PLGA/SF-loaded membranes with 3 wt% MNZ are shown in Figure 3(c). Biocompatibility is an effective way to evaluate the stimulation of materials to cells, and it is also the most direct manifestation of the influence of materials on cells [42,43]. Biocompatibility fully shows the toxicity of materials to cells [44]. PLGA has good biocompatibility [45], and the number of cells in 3 wt% MNZ/PLGA increased, which may be due to the promotion of cell growth by low concentrations of MNZ. The cells in 3 wt% MNZ/PLGA/SF 2:1 and 3 wt% MNZ/PLGA/SF 1:1 increased significantly. SF has a similar amino acid composition to human skin tissue and has good biocompatibility, which promotes cell growth [46]. At the same time, a good pore structure provides cell climbing.

3.9 Encapsulation efficiency

The encapsulation efficiency of 3 wt% MNZ/PLGA drug-loaded membranes, two groups of PLGA/SF drug-loaded

membranes containing 3 wt% MNZ at different ratios, is shown in Figure 3(d). The encapsulation efficiency indirectly indicates the ability of the delivery drug system. It can be seen that the encapsulation efficiency exceeded 85%, which is 3 wt% MNZ/PLGA of 85.63%, 3 wt% MNZ/PLGA/SF 2:1 of 93.25%, and 3 wt% MNZ/PLGA/SF 1:1 of 95.14%, respectively. Silk fibroin is a protein polymer composed of polypeptide chains of glycine and alanine repeating units, which is beneficial to the adsorption and adhesion of drugs, and promotes the encapsulation efficiency of MNZ in nanofiber membranes.

3.10 Drug release

The drug release profiles of 3 wt% MNZ/PLGA and two groups of PLGA/SF loaded membranes with 3 wt% MNZ are presented in Figure 4. The drug release behavior of the three groups of drug-loaded membranes can be categorized into two stages: an initial rapid release followed by a subsequent slow release [47]. At 1 h, the release rates of MNZ for 3 wt% MNZ/PLGA, 3 wt% MNZ/PLGA/SF 2:1, and 3 wt% MNZ/PLGA/SF 1:1 were 34.67, 42.36, and 36.56%, respectively. After 3 h, the cumulative release rates of MNZ were 42.79, 54.59, and 42.23%, respectively. At 6 h, the cumulative release rates of MNZ were 47.67, 65.14, and 54.59%, respectively. The cumulative release rates of MNZ were 53.63, 71.76, and 64.62% at 24 h and 66.27, 81.16, and 75.62% at 120 h, respectively, as the degradation entered the sustained release stage.

The initial rapid release of the drug from the nanofibers is attributed to the substantial electrokinetic force during electrospinning and the tendency of MNZ molecules to migrate toward the fiber surface. As the composite membrane enters the buffer, the burst release occurs at the contact surface between the fiber and water, causing a sharp increase in the MNZ concentration in the buffer [48]. The faster release of 3 wt% MNZ/PLGA/SF nanofiber membrane compared to 3 wt% MNZ/PLGA may be due to the hydrophilic SF dissolving in water over time, further accelerating the rapid release of the attached nanofiber membrane. The slower release of 3 wt% MNZ/PLGA/SF 1:1 compared to 3 wt% MNZ/PLGA/SF 2:1 may be because MNZ does not easily enter the buffer as the content of SF increases, causing adhesion and reducing the release rate [49]. In the sustained release stage, the drug is gradually and slowly released as the nanofiber membrane degrades, and the sustained release time can be up to 5 days. After 5 days, the drug was released continuously but slowly, which was related to the degradation of the nanofiber membrane. The degradation rate of PLGA was relatively slow, and the drug into the nanofiber membrane was also slowly and continuously released. The 3 wt% MNZ/PLGA/SF 2:1 drug-loaded membrane demonstrated superior rapid release and sustained release compared to the other two groups during drug release. After a comprehensive evaluation, the 3 wt% MNZ/PLGA/SF 2:1 drug-loaded membrane can be considered a favorable choice for periodontitis.

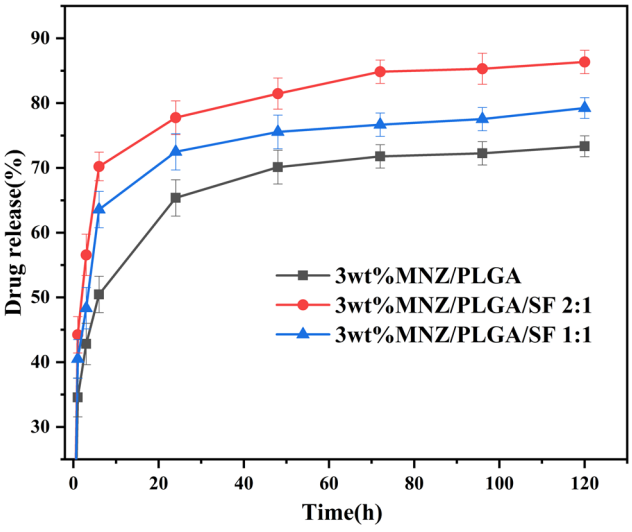

Figure 4: Drug release curves of nanofibrous membranes with different compositions.

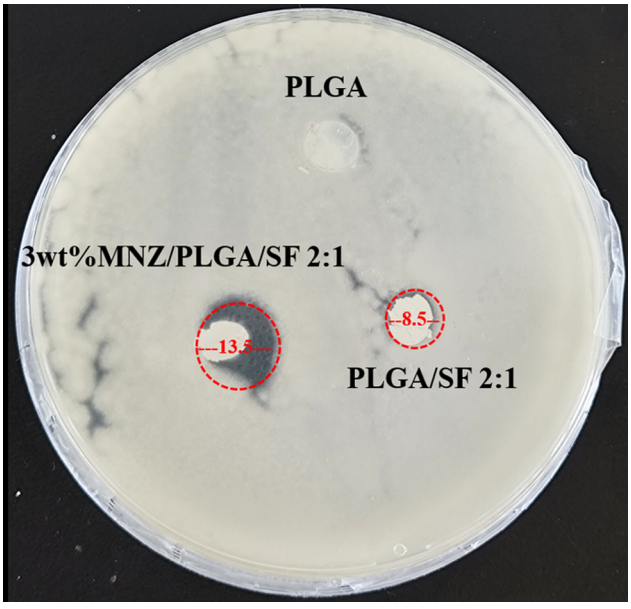

Figure 5: Antibacterial diameters of pure PLGA, 3 wt% MNZ/PLGA, and 3 wt% MNZ/PLGA/SF drug-loaded membranes.

3.11 Antibacterial test

The antibacterial properties of pure PLGA, 3 wt% MNZ/PLGA, and 3 wt% MNZ/PLGA/SF drug-loaded membranes are depicted in Figure 5. The antibacterial diameter of pure PLGA was 0 mm, indicating that pure PLGA had no antibacterial effect. The diameter of the nanofiber membrane was 8 mm, and the antibacterial diameter of PLGA/SF 2:1 was 8.5 ± 0.3 mm, suggesting that SF had a certain antibacterial effect. SF is a natural organic polymer derived from the silk gland of silkworms, and it serves a protective and antibacterial role. The antibacterial diameter of 3 wt% MNZ/PLGA/SF 2:1 was 13.5 ± 0.5 mm, indicating the successful loading of MNZ on the nanofibers and exhibiting excellent antibacterial activity. The antibacterial mechanism of MNZ involves the reduction of the nitro group in the molecule to an amino group inside the cell, inhibiting the synthesis of pathogenic DNA, and thus playing an antibacterial role [50]. The 3 wt% MNZ/PLGA/SF 2:1 exhibited outstanding antibacterial properties, effectively inhibiting bacterial growth.

4 Conclusion

The study utilized electrospinning technology to prepare MNZ/PLGA/SF nanofibers. MNZ, PLGA, and SF were physically embedded together, and each group of molecules exhibited good physicochemical properties. With the addition of MNZ, PLGA gradually changed from a hydrophobic to a hydrophilic membrane, and the hydrophilicity was enhanced with the gradual increase of SF. MNZ/PLGA/SF nanofibers demonstrated good biocompatibility and thermal stability. The results indicated that the 3 wt% MNZ/PLGA/SF 2:1 nanofibers had a better water absorption rate, *in vitro* degradation rate, and drug release compared to other groups and exhibited excellent antibacterial properties. The MNZ/PLGA/SF biomembrane shows significant potential and advantages in the treatment of periodontitis.

Acknowledgments: The authors are grateful to anonymous reviewers, whose comments improved the manuscript.

Funding information: This work was supported by the Natural Science Foundation of Sichuan Province, China (2022NSFSC1469), the Project of Chengdu Municipal Health Commission (2021059), Sichuan Province Science and Technology Transformation Project (2023ZHCG0051), Tianfu Jincheng Laboratory, City of Future Medicine project (2023ZYD0166), and Chengdu City "Unveiling and Commanding" Science and Technology Project (2024-JB00-00018-GX).

Author contributions: All authors have accepted responsibility for the entire content of this manuscript and approved its submission.

Conflict of interest: The authors state no conflict of interest.

Data availability statement: The raw/processed data required to reproduce these findings cannot be shared at this time, as the data form part of an ongoing study.

References

[1] Shin YC, Shin DM, Lee EJ, Lee JH, Kim JE, Song SH, et al. Hyaluronic acid/PLGA core/shell fiber matrices loaded with EGCG beneficial to diabetic wound healing. Adv Healthc Mater. 2016;5(23):3035–45.

[2] Chen E, Wang T, Tu Y, Sun Z, Ding Y, Gu Z, et al. ROS-scavenging biomaterials for periodontitis. J Mater Chem B. 2023;11(3):482–99.

[3] Badawi NM, Elkafrawy MA, Yehia RM, Attia DA. Clinical comparative study of optimized metronidazole loaded lipid nanocarrier vaginal emulgel for management of bacterial vaginosis and its recurrence. Drug Deliv. 2021;28(1):814–25.

[4] Shokrolahi F, Latif F, Shokrollahi P, Farahmandghavi F, Shokrollahi S. Engineering atorvastatin loaded Mg-Mn/LDH nanoparticles and their composite with PLGA for bone tissue applications. Int J Pharm. 2021;606:120901.

[5] Jentsch HF, Dietrich M, Eick S. Non-surgical periodontal therapy with adjunctive amoxicillin/metronidazole or metronidazole when no aggregatibacter actinomycetemcomitans is detected—a randomized clinical trial. Antibiotics. 2020;9(10):686.

[6] Budai-Szűcs M, Léber A, Cui L, Józó M, Vályi P, Burián K, et al. Electrospun PLA fibers containing metronidazole for periodontal disease. Drug Des Dev Ther. 2020;14:233–42.

[7] Liu Z, Shang S, Chiu K-L, Jiang S, Dai F. Fabrication of silk fibroin/poly (lactic-co-glycolic acid)/graphene oxide microfiber mat *via* electrospinning for protective fabric. Mater Sci Eng: C. 2020;107:110308.

[8] Mirzaeei S, Mansurian M, Asare-Addo K, Nokhodchi A. Metronidazole-and amoxicillin-loaded PLGA and PCL nanofibers as potential drug delivery systems for the treatment of periodontitis: *in vitro* and in vivo evaluations. Biomedicines. 2021;9(8):975.

[9] Meng Z, Li H, Sun Z, Zheng W, Zheng Y. Fabrication of mineralized electrospun PLGA and PLGA/gelatin nanofibers and their potential in bone tissue engineering. Mater Sci Eng: C. 2013;33(2):699–706.

[10] Wu S, Zhou R, Zhou F, Streubel PN, Chen S, Duan B. Electrospun thymosin Beta-4 loaded PLGA/PLA nanofiber/microfiber hybrid yarns for tendon tissue engineering application. Mater Sci Eng: C. 2020;106:110268.

[11] Li G, Wang J, Xu M, Zhang H, Tu C, Yang J, et al. Engineered exosome for NIR-triggered drug delivery and superior synergistic chemo-phototherapy in a glioma model. Appl Mater Today. 2020;20:100723.

[12] Nagiah N, Murdock CJ, Bhattacharjee M, Nair L, Laurencin CT. Development of tripolymeric triaxial electrospun fibrous matrices for dual drug delivery applications. Sci Rep. 2020;10(1):609.

[13] Kwak S, Haider A, Gupta KC, Kim S, Kang I-K. Micro/nano multilayered scaffolds of PLGA and collagen by alternately electrospinning for bone tissue engineering. Nanoscale Res Lett. 2016;11:1–16.

[14] Liu S, Kau Y, Chou C, Chen J, Wu R, Yeh W. Electrospun PLGA/collagen nanofibrous membrane as early-stage wound dressing. J Membr Sci. 2010;355(1–2):53–9.
[15] Zhao W, Li J, Jin K, Liu W, Qiu X, Li C. Fabrication of functional PLGA-based electrospun scaffolds and their applications in biomedical engineering. Mater Sci Eng: C. 2016;59:1181–94.
[16] Ma Y, Song J, Almassri HN, Zhang D, Zhang T, Cheng Y, et al. Minocycline-loaded PLGA electrospun membrane prevents alveolar bone loss in experimental peridontitis. Drug Deliv. 2020;27(1):151–60.
[17] Liu Z, Shang L, Ge S. Immunomodulatory effect of dimethyloxallyl glycine/nanosilicates-loaded fibrous structure on periodontal bone remodeling. J Dental Sci. 2021;16(3):937–47.
[18] Wei Y, Liu Z, Zhu X, Jiang L, Shi W, Wang Y, et al. Dual directions to address the problem of aseptic loosening *via* electrospun PLGA@aspirin nanofiber coatings on titanium. Biomaterials. 2020;257:120237.
[19] Xie M. Volumetric additive manufacturing of pristine silk-based (bio) inks. Nat Commun. 2023;14(1):210.
[20] Wang J, Yang Q, Cheng N, Tao X, Zhang Z, Sun X, et al. Collagen/silk fibroin composite scaffold incorporated with PLGA microsphere for cartilage repair. Mater Sci Eng: C. 2016;61:705–11.
[21] Zhu J, Luo J, Zhao X, Gao J, Xiong J. Electrospun homogeneous silk fibroin/poly (ε-caprolactone) nanofibrous scaffolds by addition of acetic acid for tissue engineering. J Biomater Appl. 2016;31(3):421–37.
[22] Xie X, Yu J, Zhao Z, Zheng Z, Xie M, Wang X, et al. Fabrication and drug release properties of curcumin-loaded silk fibroin nanofibrous membranes. Adsorpt Sci Technol. 2019;37(5–6):412–24.
[23] Liua Q, Zhoua S, Zhao Z, Wua T, Wang R. SF/polyethylene glycol nano-fibrous membranes loaded with curcumin. Therm Sci. 2017;21(4):1587–94.
[24] Zhang L, Wang Z, Xiao Y, Liu P, Wang S, Zhao Y, et al. Electrospun PEGylated PLGA nanofibers for drug encapsulation and release. Mater Sci Eng: C. 2018;91:255–62.
[25] Chen H, Lin M. Characterization, biocompatibility, and optimization of electrospun SF/PCL/CS composite nanofibers. Polymers. 2020;12(7):1439.
[26] Li J, Zhu J, He T, Li W, Zhao Y, Chen Z, et al. Prevention of intra-abdominal adhesion using electrospun PEG/PLGA nanofibrous membranes. Mater Sci Eng: C. 2017;78:988–97.
[27] Mehrasa M, Asadollahi MA, Ghaedi K, Salehi H, Arpanaei A. Electrospun aligned PLGA and PLGA/gelatin nanofibers embedded with silica nanoparticles for tissue engineering. Int J Biol Macromol. 2015;79:687–95.
[28] Xie X, Shi X, Wang S, Cao L, Yang C, Ma Z. Effect of attapulgite-doped electrospun fibrous PLGA scaffold on pro-osteogenesis and barrier function in the application of guided bone regeneration. Int J Nanomed. 2020;15:6761–77.
[29] Mehrasa M, Asadollahi MA, Nasri-Nasrabadi B, Ghaedi K, Salehi H, Dolatshahi-Pirouz A, et al. Incorporation of mesoporous silica nanoparticles into random electrospun PLGA and PLGA/gelatin nanofibrous scaffolds enhances mechanical and cell proliferation properties. Mater Sci Eng: C. 2016;66:25–32.
[30] Miao H, Shen R, Zhang W, Lin Z, Wang H, Yang L, et al. Near-infrared light triggered silk fibroin scaffold for photothermal therapy and tissue repair of bone tumors. Adv Funct Mater. 2021;31(10):2007188.
[31] Qian Y, Zhou X, Zhang F, Diekwisch TG, Luan X, Yang J. Triple PLGA/PCL scaffold modification including silver impregnation, collagen coating, and electrospinning significantly improve biocompatibility, antimicrobial, and osteogenic properties for orofacial tissue regeneration. ACS Appl Mater Interfaces. 2019;11(41):37381–96.
[32] Yan W, Chen Y, Han L, Sun K, Song F, Yang Y, et al. Pyrogenic dissolved organic matter produced at higher temperature is more photoactive: Insight into molecular changes and reactive oxygen species generation. J Hazard Mater. 2022;425:127817.
[33] Yang J, Zhang T, Cai J, Niu B, Zhang Y, Long D. Investigating the pyrolysis mechanisms of three archetypal ablative resins through pyrolysis experiments and ReaxFF MD simulations. Mater Today Commun. 2023;36:106683.
[34] Yao J, Liu Z, Ma W, Dong W, Wang Y, Zhang H, et al. Three-dimensional coating of SF/PLGA coaxial nanofiber membranes on surfaces of calcium phosphate cement for enhanced bone regeneration. ACS Biomater Sci Eng. 2020;6(5):2970–84.
[35] Wu L, Li H, Li S, Li X, Yuan X, Li X, et al. Composite fibrous membranes of PLGA and chitosan prepared by coelectrospinning and coaxial electrospinning. J Biomed Mater Res Part A: Off J Soc Biomater Jpn Soc Biomater Aust Soc Biomater Korean Soc Biomater. 2010;92(2):563–74.
[36] Qiu H, Zhu S, Pang L, Ma J, Liu Y, Du L, et al. ICG-loaded photodynamic chitosan/polyvinyl alcohol composite nanofibers: Anti-resistant bacterial effect and improved healing of infected wounds. Int J Pharm. 2020;588:119797.
[37] Liu X, Hou P, Liu S, Qi J, Feng S, Zhang L, et al. Effect of poly (lactic-co-glycolic acid) blend ratios on the hydrolytic degradation of poly (para-dioxanone). J Polym Res. 2021;28:1–11.
[38] Zhu Y, Song F, Ju Y, Huang L, Zhang L, Tang C, et al. NAC-loaded electrospun scaffolding system with dual compartments for the osteogenesis of rBMSCs *in vitro* [Erratum]. Int J Nanomed. 2019;14:1705–6.
[39] Zhu Y, Wang Z, Li L, Gao D, Xu Q, Zhu Q, et al. *In vitro* degradation behavior of a hydroxyapatite/poly (lactide-co-glycolide) composite reinforced by micro/nano-hybrid poly (glycolide) fibers for bone repair. J Mater Chem B. 2017;5(44):8695–706.
[40] Lee D, Heo DN, Lee SJ, Heo M, Kim J, Choi S, et al. Poly (lactide-co-glycolide) nanofibrous scaffolds chemically coated with gold-nanoparticles as osteoinductive agents for osteogenesis. Appl Surf Sci. 2018;432:300–7.
[41] Jin S, Sun F, Zou Q, Huang J, Zuo Y, Li Y, et al. Fish collagen and hydroxyapatite reinforced poly (lactide-co-glycolide) fibrous membrane for guided bone regeneration. Biomacromolecules. 2019;20(5):2058–67.
[42] Yang F, Wang J, Li X, Jia Z, Wang Q, Yu D, et al. Electrospinning of a sandwich-structured membrane with sustained release capability and long-term anti-inflammatory effects for dental pulp regeneration. Bio-Des Manuf. 2022;5(2):305–17.
[43] Yang J, Li G, Yuan J, Jing S, Wang X, Yang F, et al. A smart silk-based microneedle for cancer stem cell synergistic immunity/hydrogen therapy. Adv Funct Mater. 2022;32(41):2206406.
[44] Foraida ZI, Kamaldinov T, Nelson DA, Larsen M, Castracane J. Elastin-PLGA hybrid electrospun nanofiber scaffolds for salivary epithelial cell self-organization and polarization. Acta Biomater. 2017;62:116–27.
[45] Díaz E, Puerto I, Ribeiro S, Lanceros-Mendez S, Barandiarán JM. The influence of copolymer composition on PLGA/nHA scaffolds' cytotoxicity and *in vitro* degradation. Nanomaterials. 2017;7(7):173.
[46] Wu T, Li D, Wang Y, Sun B, Li D, Morsi Y, et al. Laminin-coated nerve guidance conduits based on poly (l-lactide-co-glycolide) fibers and

yarns for promoting Schwann cells' proliferation and migration. J Mater Chem B. 2017;5(17):3186–94.
[47] Spadaro S, Santoro M, Barreca F, Scala A, Grimato S, Neri F, et al. PEG-PLGA electrospun nanofibrous membranes loaded with Au@ Fe 2 O 3 nanoparticles for drug delivery applications. Front Phys. 2018;13:1–9.
[48] Peng Y, Ma Y, Bao Y, Liu Z, Chen L, Dai F, et al. Electrospun PLGA/SF/artemisinin composite nanofibrous membranes for wound dressing. Int J Biol Macromol. 2021;183:68–78.
[49] Boncu TE, Guclu AU, Catma MF, Savaser A, Gokce A, Ozdemir N. *In vitro* and in vivo evaluation of linezolid loaded electrospun PLGA and PLGA/PCL fiber mats for prophylaxis and treatment of MRSA induced prosthetic infections. Int J Pharm. 2020;573:118758.
[50] de Paula Zago LH, de Annunzio SR, de Oliveira KT, Barbugli PA, Valdes BR, Feres M, et al. Antimicrobial photodynamic therapy against metronidazole-resistant dental plaque bactéria. J Photochem Photobiol B: Biol. 2020;209:111903.